Theor Chem Acc (2002) 108:273–285
DOI 10.1007/s00214-002-0366-6

Theoretical
Chemistry Accounts

Feature article

Signatures of reactive resonance: three case studies

Sheng Der Chao, Rex T. Skodje

Department of Chemistry and Biochemistry, University of Colorado, Boulder, CO 80309, USA

Received: 2 March 2002 / Accepted: 2 June 2002 / Published online: 17 October 2002

Abstract. Recent advances in the study of short-lived reactive resonances are reviewed. Special emphasis is given to addressing the question of how reactive resonances might be observed in molecular beam scattering experiments. Three case studies are presented for simple triatomic systems that are believed to exhibit resonance phenomena: $F + HD \rightarrow D + HF$, $F + H_2 \rightarrow H + HF$, and $H + HD \rightarrow D + H_2$. It is seen that reactive resonances do strongly influence collision observables, but in a different way for each case. At this stage, there does not appear to be a unique resonance signature that can be applied to all reactions.

Key words: Resonance – Molecular beams – Reaction dynamics

1 Introduction

It is widely appreciated that many important chemical reactions do not proceed directly through the transition-state region, but instead form intermediate reactive complexes that subsequently decay into the final reaction products [1]. For certain classes of reactions, the occurrence of reactive complexes is completely predictable on the basis of the existence of deep potential-energy wells along the reaction coordinate. Ion–molecule reactions, such as $D^+ + H_2 \rightarrow HD^+ + H$, and insertion-type reactions, such as $O(^1D) + H_2 \rightarrow OH + H$, are well-known cases in point. For deep-well trapping, the complex lifetimes are typically tens or hundreds of periods of internal vibration, and thus the complexes are well-defined species. On the other hand, complexes are also believed to occur for systems where the potential-energy surface (PES) is purely (or dominantly) repulsive, although they are much more unstable [2, 3, 4, 5]. In such systems, which include a number of hydrogen-abstraction-type reactions, the origin of trapping near the transition state is dynamical and is not obvious from the landscape of the PES. The lifetimes of these intermediates are often just a few or merely one internal vibrational period. Despite their transitory existence, these "reactive resonances" can have a strong influence on both the rate of the reaction and the resulting product distribution. On a more fundamental level, the characteristics of the reactive complexes, such as energy level spacing and lifetimes, provide important information about the PES and the dynamics near the critical transition-state region.

The existence and characteristics of short-lived reactive resonances has been the subject of much discussion over the years. Many of the early advances in this field were made from the analysis of quantum reaction dynamics on approximate PESs [6, 7, 8, 9, 10, 11]. These studies provided much insight into the dynamical origin of complex formation, but were speculative in that the PES and the dynamics calculations were too approximate to permit quantitative comparisons with experiment. With the dramatically increased computational power now available, theory has evolved to the point where very accurate potential surfaces and essentially converged quantum scattering calculations can be used to predict the existence of reactive resonances a priori for sufficiently simple systems [12, 13, 14, 15]. Furthermore, techniques of analysis have been developed that allow the resonance wavefunction to be extracted and, hence, the full assignment of quantum numbers and other physical characteristics [16, 17, 18, 19].

On the other hand, the experimental search for reactive resonances has proven a much more stubborn problem. For some reactions, transition-state spectroscopy can be employed to study resonances as "half-collision experiments" where even very short lived resonances may be observed [20]. Weaver et al. [21] were able to assign peaks in the $[IHI]^-$ photodetachment spectrum to resonance states for the neutral I + HI reaction. Unfortunately, transition-state spectroscopy is

Correspondence to: R. T. Skodje
e-mail: skokje@spot.colorado.edu

not always feasible, owing to the absence of an appropriate Franck–Condon transition or to practical limitations in the required level of energetic resolution. The direct study of reactive resonances in a full-collision experiment, such as with a molecular beam apparatus, is the traditional and more universal environment in which to work. Unfortunately, observing resonance behavior in such experiments has proven to be exceedingly difficult. The heart of problem is not a technical experimental issue, but rather it is a lack of knowledge about how the existence of a resonance will affect the collision observables in a uniquely identifiable way. As of this point, there is no known general and unique resonance signature that can be sought, even given perfectly resolved scattering cross section data.

In this article, we review recent advances that have been made in detecting and understanding short-lived reactive resonances. Theory and experiment have matured to the point where state- and angle-resolved reactive cross sections can be measured accurately in the laboratory and brought into quantitative agreement with the results of converged scattering calculations on an accurate PES. We attempt to illustrate how theory and experiment can work in tandem to identify resonance signatures in reactive collisions. A brief discussion of the theory of reactive resonances is presented in Sect. 2, with special emphasis given to how collision observables are affected by the existence of a resonance. We present three case studies of systems where reactive resonances are believed to exist in Sect. 3: F + HD, F + H_2, and H + HD. Although these three hydrogen abstraction reactions are seemingly quite similar, we shall see that, in fact, the resonance signatures are very different in each case. We are thus led to the conclusion that the search for resonance signatures in collision experiments must still be pursued on a case-by-case basis with close interplay between theory and experiment. Finally, we present a brief conclusion in Sect. 4.

2 The theory of reactive resonances

In this section we discuss the theory of reactive resonances for systems described by a single Born–Oppenheimer PES that exhibits no deep trapping wells. We review the dynamical picture of resonance trapping, as well as several techniques for extracting resonance properties using quantum dynamics methods. The main discussion addresses the practical issue of how the existence of resonances should affect scattering observables.

In the absence of a trapping well on the PES, the existence of resonances is tied to the characteristics of the effective dynamical potential, which includes some aspects of the coupling between modes of the collision complex and provides a model for dynamical trapping. The most common approach is through the use of vibrationally adiabatic theory [22, 23], There, one defines a reaction coordinate, s, and orthogonal vibrational modes, $\boldsymbol{u}$, along the reaction pathway. If the vibrational quantum numbers, $\boldsymbol{n}$, of the $\boldsymbol{u}$ motion are assumed to be conserved, a vibrationally adiabatic dynamical potential can be constructed as

$$V_{\mathrm{ad}}(s;\boldsymbol{n}) = V_0(s) + \varepsilon_{\boldsymbol{n}}(s) \ , \tag{2.1}$$

where $V_0(s)$ is the potential along the reaction path and $\varepsilon_{\boldsymbol{n}}(s)$ are the quantized state energies of the orthogonal motion. Since the vibrational frequencies change dramatically near the transition state, $V_{\mathrm{ad}}(s;\boldsymbol{n})$ can be quite different from the Born–Oppenheimer surface, and can even exhibit wells although the PES is purely repulsive. Although the dynamical conditions for the technical validity of the vibrationally adiabatic model are virtually never satisfied, this simple model often captures the essence of reaction dynamics near the transition state.

The two most common scenarios for resonance trapping can be summarized as follows:

1. Adiabatic well trapping. Resonance states can exist as intermediates trapped in wells on the adiabatic potential curves, as shown in the upper panel of Fig. 1. This requires the adiabatic wells to be deep enough to support a quantum state, which generally occurs only for internally excited complexes. The decay of the resonance can take place either by tunneling through the barrier, or by energy transfer resulting in a transition to a lower adiabatic curve. The lifetime of the resonance depends strongly on the vibrationally nonadiabatic coupling and tends to be the longest for heavy–light–heavy mass combinations.
2. Barrier trapping. Even when there is no well in $V_{\mathrm{ad}}(s;\boldsymbol{n})$, it is possible to show that trapping occurs

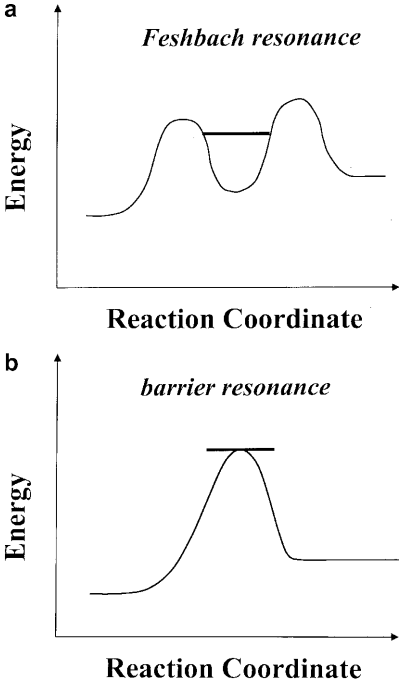

Fig. 1. A schematic diagram showing how adiabatic potential curves can support reactive resonances. The *upper panel* shows the conventional Feshbach resonance trapped in a well of an adiabatic curve. The *lower panel* illustrates barrier trapping, which occurs near the energy of the barrier maximum of an adiabatic curve

near the barrier maximum simply because the motion slows down while passing over the barrier, as in the lower panel of Fig. 1 [1, 24, 25]. This sort of kinematic trapping occurs even in classical mechanics and is related to the existence of a periodic orbit perched on top of the dynamical barrier [17, 26, 27, 28]. Although there are some important differences between "barrier-states" and more conventional Feshbach resonances, it can be shown [17, 24, 25, 29, 30, 31] that barrier-states behave much like resonances with energy $E_{\rm res} = V_{\rm ad}(s = \text{barrier};\boldsymbol{n})$ and width $\Gamma = \hbar\omega$, with ω being the barrier frequency of $V_{\rm ad}(s;\boldsymbol{n})$. The lifetimes of barrier-states are typically about one period of vibration for the u coordinates even if ω should happen to be (accidentally) small.

While vibrationally adiabatic theory provides a reasonable physical picture for dynamical resonances in chemical reactions, it is necessary to adopt a more exact treatment of the quantum dynamics to extract accurate resonance properties. Real or complex stabilization calculations have been traditionally employed to compute resonances in reactive problems [32, 33]. More recently, complex continuation of the resolvent has been shown to provide a robust scheme to compute resonance positions and widths [19]. Diagonalizing the Hamiltonian in an L^2 basis with an imaginary absorbing potential to impose boundary conditions can also be used to obtain resonances [34]. We have found [14, 16, 17] that the spectral quantization (SQ) method [35, 36] provides a very satisfactory method to compute the properties of broad reactive resonances. In this technique, the resonance wavefunction is obtained from the Fourier transform time-dependent wavepacket that has been variationally optimized to reduce the contribution of nonresonant direct scattering.

When couched in the language of scattering theory [37] intermediate reactive complexes for gas-phase reactions can be taken as examples of quantum resonance phenomena. This viewpoint is quite useful since it provides a collection of generic behavior that guides both experimental and theoretical studies. The standard picture of resonance phenomena is based on the concept of the isolated narrow resonance (INR) proposed by Breit and Wigner [38]. The INR is pictured as a "nearly bound" state of the system lying at energies above the threshold for complex breakup, i.e., in the continuum region of the energy spectrum. In the Breit–Wigner treatment, the fundamental characteristic of the INR is the existence of a complex energy pole in the scattering matrix (**S** matrix), i.e.,

$$\mathbf{S}(E) = \mathbf{S}_{\rm d}(E)\left(1 - \frac{i\mathbf{A}}{E - E_{\rm R} + i\Gamma/2}\right) \ , \tag{2.2}$$

where $E_{\rm R}$ is the (real) resonance energy and Γ is the total width [39]. In Eq. (2.2), $\mathbf{S}_{\rm d}(E)$ is the direct, or background, contribution, which is assumed to be a slowly varying function of the total system energy, E. The matrix **A** is composed of the partial widths of the resonance according to

$$A_{i,j} = \gamma_i^* \gamma_j \ , \tag{2.3}$$

with $\Gamma_i = |\gamma_i|^2$, that in turn satisfies

$$\Gamma = \sum_i \Gamma_i \ , \tag{2.4}$$

where the indices label the open channels. For an INR, the complex energy,

$$z = E_{\rm R} - i\Gamma/2 \ , \tag{2.5}$$

is assumed to lie very close to the real axis, i.e., Γ is small, so the background contribution to $\mathbf{S}(E)$ may be readily separated from the resonance pole. Furthermore, it is assumed that no other pole of the **S** matrix lies nearby in energy as defined on the scale set by Γ. When these conditions are met, the existence of a resonance is heralded by the occurrence of set of well-defined effects that are amenable to observation or computation.

1. Resonance peaks in integral cross sections (ICS). The most dramatic manifestation of an INR is the appearance of a narrow feature in the ICS, $\sigma(E)$ at total energy $E = E_{\rm R}$ of width Γ. Depending on the relative phase of the direct and resonant contributions, the feature may appear as a peak, a dip, or a more general combination of the two. The resonance feature should occur at the same total energy for all state-to-state ICS, with the relative heights set by the partial widths. By assumption, the resonance will occur for just one value of the total angular momentum, J, while any companion resonances for other J are well isolated in energy.
2. Exponential decay of a prepared state. Associated with the pole of the **S** matrix is a Seigert state, $\Psi_{\rm res}$, which has purely outgoing boundary conditions and satisfies (with some caveats) the equation, $\mathbf{H}\Psi_{\rm res} = z\Psi_{\rm res}$, **H** being the system Hamiltonian [40]. If a square integrable approximation to $\Psi_{\rm res}$ is constructed, then its time evolution, $\Psi_{\rm res}(t)$, will exhibit pure exponential decay after a transient induction period. Thus, a sample of prepared "complex" molecules will deplete according to the law, $N(\mathrm{t}) = N(0)\mathrm{e}^{-\mathrm{t}/\tau}$, where the lifetime τ is related to the resonance width according to $\tau = \hbar/\Gamma$. Furthermore, the decay flux into each outgoing channel is locked in fixed proportion at all times.
3. Dramatic shifts in angular distributions. If the scattering process consists of contributions from a number of partial waves, then the angular dependence of the differential cross sections (DCS), $\mathrm{d}\sigma/\mathrm{d}\Omega$, will generally change rapidly around the resonance energy as one partial wave becomes greatly enhanced. One expects the resonant contribution to $\mathrm{d}\sigma/\mathrm{d}\Omega$ will be forward–backward symmetric [41].
4. Time delay. Since resonances are always associated with dynamical trapping, the collision time, relative to a reference system with no scattering potential, should exhibit a large positive peak at the resonance energy. This time delay can be quantified from the shift in the center of a wavepacket, as suggested by Wigner and Eisenbud [42], or through the time-delay matrix formulated by Smith [43]. The angle-resolved time delay was formulated by Goldberger and coworkers [44], and later by Kuppermann and Wu [45].

5. Product distributions. The branching ratios into the various product channels, such as the allowed rovibrational states, will generally be different for the direct scattering compared to the resonance decay. Thus, one expects to see a rapid variation in the branching ratios as the resonance energy is scanned.

The INR concept has succeeded beautifully for many problems in atomic and nuclear physics, where the various resonance signatures have been unambiguously observed or calculated. Unfortunately, the INR picture is seldom valid for reactive resonances, which, in contrast, tend to be broad and overlapping. As a consequence, the resonance signatures just outlined must be dramatically modified or totally abandoned, and we are left with an open question of how a reactive resonance may be detected in a collision experiment. The breakdown of the INR idealization for reactive resonances was appreciated long ago in terms of the impact parameter averaging implicit in reactive collisions [46]. If we imagine that an "isolated" reactive resonance corresponds to a vibrational state of an intermediate molecule, then the rotational energy levels built on that state have energies given by

$$E_{\mathrm{res}}(J) = E_0 + B_0 J(J+1) \ , \tag{2.6}$$

where E_0 is the ground rotational energy and B_0 is the rotation constant of the complex. (For simplicity, we have specialized to the case of a collinear collision complex.) Hence, each resonance state is part of a rotational progression with spacing $2JB_0$. The typical B constant for a reactive resonance can be inferred from the geometry of the saddle point on the PES and is usually of the order of several wavenumbers. On the other hand, the resonance lifetimes tend to be less than 100 fs, corresponding to widths of more than 50 cm^{-1} and thus the rotational states overlap. The state-to-state reaction probabilities (averaged over helicity, i.e., the projection of the internal angular momentum along the translational velocity) at fixed J, $P_{\mathrm{R}}(v, j \to v', j'; E_{\mathrm{C}}, J)$, may show Lorentzian peaks at resonances, but the experimental observable is the cross section:

$$\sigma_{\mathrm{R}}(v,j \to v',j';E_{\mathrm{C}}) = \frac{\pi}{k^2} \sum_J (2J+1) \cdot P_{\mathrm{R}}(v,j \to v',j';E_{\mathrm{C}},J) \ , \tag{2.7}$$

where k is the incident wavevector, which is related to the collision energy, E_{C}, by $k = \sqrt{2\mu E_{\mathrm{C}}}/\hbar$. Since reactive cross sections generally involve dozens of partial waves, even for low collision energy, the scattering amplitudes at a single energy will reflect the contribution of many states of the progression and clear resonance signatures tend to be washed out by averaging. Stated in dynamical terms, the rotation period of the complex is significantly greater than the lifetime of the resonance.

In light of the preceding discussion, it is clear that the unmistakable resonance fingerprint provided by a narrow Lorentzian peak in the ICS will seldom be observed for reactive resonance in a collision experiment. Similarly, sharp structure versus energy in the product state and angular distributions will also tend to be smeared over energy by the impact parameter averaging. Of course, in a theoretical calculation we can investigate one partial wave at a time and thus resonances may still be identified by time-delay analysis or by direct calculation of the Seigert state using, for example, the SQ method. Unfortunately, the experimentalist does not have this luxury and the resonance signature must be sought in the impact-parameter-averaged cross sections.

In place of the INR predictions, several ideas have been proposed for detecting reactive resonances. Miller and Zhang suggested searching for a ridge structure in the DCS as a function of E_{C} and θ. The ridge is an E_{C}–θ correlation resulting from the J-shifting of the dominant resonance decay angle in the DCS. Miller and Zhang [47], observed ridge structures in the H + H_2 and D + H_2 systems; however, it is unclear whether ridge structures uniquely correlate to quantum resonances since Aoiz et al. [48] have noted similar ridges occur in quasiclassical trajectory (QCT) simulations. Neumark and coworkers [49, 50] surmised that forward peaks in the state-resolved DCS might indicate the existence of resonances. The physical picture behind this idea is somewhat subtle and involves resonant time delay. As the impact parameter (or J) of the collision increases, the total reactive product distribution generally shifts from backward to more sideways scattering, reflecting the orientation of the complex. One expects that the resonant contribution to the product distribution will show greater angular deflection (toward forward) since the complex will rotate further owing to the time delay. Thus, in the most forward direction, the dynamics will be filtered to enhance the resonant contribution to the reaction. Forward peaks have in fact been observed in the F + H_2 [49], H + D_2 [51, 52, 53], and H + HD [54] reactions. Finally, we note that it would not be unreasonable to expect that resonances may give rise to other "unusual" structures in the state- and angle-resolved DCS as a function of collision energy since the state and angle resolution effectively undoes part of the effect of impact parameter averaging.

3 Three case studies

In order to assess the utility of various ideas for resonance signatures, in this section we consider three case studies of benchmark chemical reactions believed to support reactive resonances. These are the hydrogen exchange reactions: F + HD → HF + D, F + H_2 → HF + H, and H + HD → D + H_2. For each case, state-of-the-art molecular beam experiments have recently been carried out. Furthermore, very accurate PESs have also been computed for these reactions, which have been used to perform converged quantum scattering calculations. Each of these systems is a triatomic hydrogen abstraction reaction dominated by the lowest PES that exhibits no potential well near the transition state. One might hope that a common resonance fingerprint might be found for these reactions. On the contrary, we shall see that presence of resonances is manifested in different observables for each case. The chameleon-like nature of the resonance emphasizes the need for combined theoretical

and experimental work to firmly establish the resonance on a case-by-case basis.

3.1 F + HD → HF + D, a clear resonance

The first clear observation of a reactive resonance in a collision experiment was recently made for the F + HD → HF + D reaction [55, 56, 57]. This reaction was one isotopomer of the F + H_2 system studied in the landmark molecular beam experiments of Neumark et al. in 1985 [50]. Unlike the F + H_2 case, the anomalous forward peaking of the product molecules was not well resolved, and the results for F + HD were described as the most classical-like of the isotopes considered. Furthermore, a detailed quantum mechanical study [58] of the F + HD → HF + D reaction on the accurate Stark–Werner (SW) PES [59], failed to locate resonance states. Therefore, it was surprising that the unmistakable resonance fingerprints emerged so clearly upon re-examination of this reaction.

The molecular beam experiments of Skodje et al. [55, 56] employed the Doppler profile time-of-flight technique that allowed the ready observation of the excitation function (i.e., the total reactive ICS summed over the final product state) at many collision energies for a HD reagent molecule 90% populated in its ground ro-vibrational state. The excitation function for both possible product channels, HF + D and DF + H, over the range of collision energies 0.2–3 kcal mol^{-1} is shown in Fig. 2. A pronounced step-like feature that is clearly absent for the DF + H channel occurs in $\sigma_R(E)$ for the HF + D channel near $E_C = 0.5$ kcal mol^{-1}. A converged quantum scattering calculation [55, 56, 60] on the SW PES is found to yield similar results, as seen in the figure. The QCT results of Aoiz et al. [61] showed reasonable agreement with experiment for the H + FD channel, but completely failed to predict the step feature for the D + HF product. Since the step occurs below the adiabatic barrier, one is led to the conclusion that the reaction step is due to quantum effects. With close interaction between theory and experiment, the interpretation that emerged [55, 56] for this result was that the reactive step was due to the existence of a reactive resonance with a F–H–D collinear geometry. The step was not seen in the DF + H channel since the decay probability of an F–H–D configured resonance was very small in this unfavorable product channel. The difference in the step height predicted by quantum scattering and that observed in the experiment is probably due to small errors in the SW PES affecting the rate of resonant tunneling.

In light of the preceding discussion, it is very surprising that a clear resonant feature should survive in $\sigma_R(E)$, which, after all, involves averaging over the impact parameter, the scattering angle, and the final states. Some insight into this result is obtained by considering the partial cross sections computed for the individual partial waves that are shown in Fig. 3. As a function of E_C, each of the partial cross sections shows a clear Lorentzian-like peak at low E_C followed by the normal

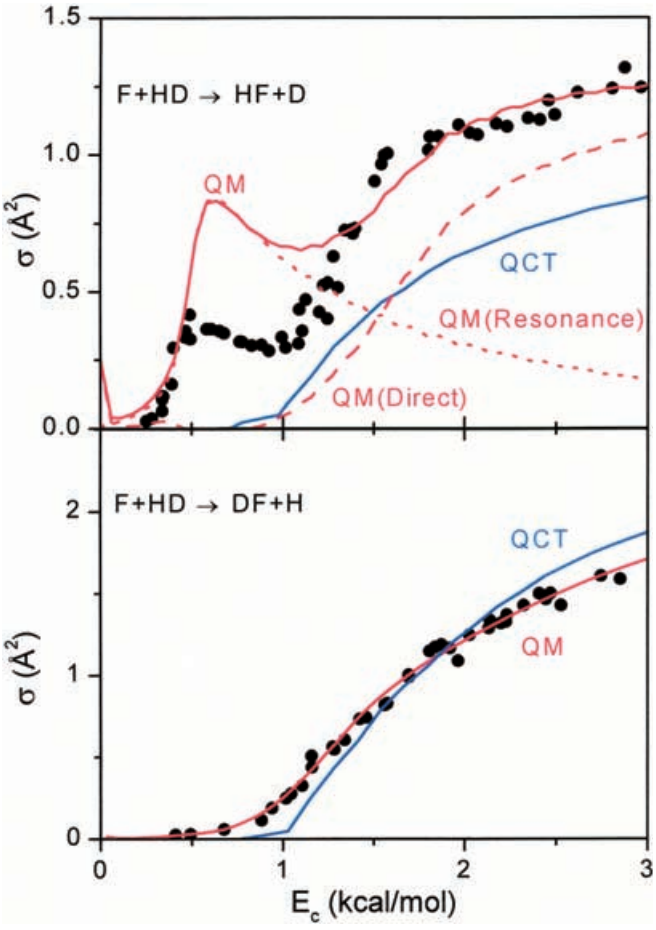

Fig. 2. The normalized excitation functions versus collision energy for the two isotopic channels for the F + HD reaction. The *solid line* is the result of quantum scattering theory using the Stark–Werner (*SW*) potential-energy surface (*PES*). The quasiclassical trajectory (*QCT*) simulations from Ref. [61] are plotted for comparison. The experimental results, shown by *points*, are normalized to theory by a single scaling factor for both channels. Also shown in the *upper panel* is the theoretical decomposition of the excitation function into direct and resonant contributions using the *J*-shifting procedure

threshold-type behavior at higher E_C. The individual peaks fit well to a Lorentzian shape function with peak positions at

$$E_{res}(J) = E_0 + B_0 J(J+1) \ , \tag{3.1}$$

with $E_0 = 0.52$ kcal mol^{-1} and $B_0 = 0.0051$ kcal mol^{-1}, and widths given by the fitted form

$$\Gamma(J) = \Gamma_0 + a[\exp(bJ) - 1] \ , \tag{3.2}$$

with $\Gamma_0 = 0.15$ kcal mol^{-1}, $a = 0.00127$ kcal mol^{-1}, and $b = 0.2635$. Since the threshold energy for the "direct" F + HD → HF + D reaction obtained from the lowest vibrationally adiabatic barrier is at about 1.1 kcal mol^{-1}, the reactive step in $\sigma_R(E)$ is due almost entirely to the superposition of the Lorentzian peaks. Indeed, by numerically decomposing the partial cross sections into separate peak and direct contributions, and then summing over J to obtain $\sigma_R(E)$, we see in Fig. 2 that the step is essentially the J-shifted analog of a pure

Lorentzian peak. Schatz et al. [62] conjectured that such a step might exist in an approximate analysis of the Cl + HCl reaction. If the Lorentzian feature is indeed taken as a resonance peak, this implies that the reaction occurs almost exclusively as resonance mediated tunneling at energies below about 1 kcal mol^{-1}.

The quantum product state distributions from the reaction show a similar dichotomy for $E_C < 1$ kcal mol^{-1} and $E_C > 1$ kcal mol^{-1}. Focusing on the rotational state distribution for the dominant HF ($v' = 2$) product, in Fig. 4 we show the ICS for F + HD $\rightarrow$ HF($v' = 2$,j') + D as a function of j' and E_C. The scattering calculations show a clear change in the rotational product distribution between low- and high-energy scattering. The rotational distribution at low E_C is rather flat, yet hot extending up to about $j' = 10$. By contrast, the higher E_C results show the more usual envelope peaking at much lower values of j'. Recently, Harper et al. [63] measured the product distribution in a "crossed-jet" experiment and obtained results consistent with Fig. 4. Again, the result is consistent with a resonance state picture in that the low E_C distribution is due entirely to a resonance decay mechanism that is expected to be quite different from the direct reaction mechanism that dominates at higher E_C.

The DCS for the F + HD $\rightarrow$ HF + D reaction is also imprinted with resonance signatures. In Fig. 5, we show the DCS versus E_C and θ, for the HF($v' = 2$) + D product, summed over j' states, obtained experimentally and theoretically. At low collision energies, a resonance ridge of the sort proposed by Miller and Zhang [47] is clearly apparent. The product distribution is backward-peaked at the lowest energy, and then shifts progressively toward the sideways direction. At high E_C, the DCS develops strong forward/backward peaking. A decom-

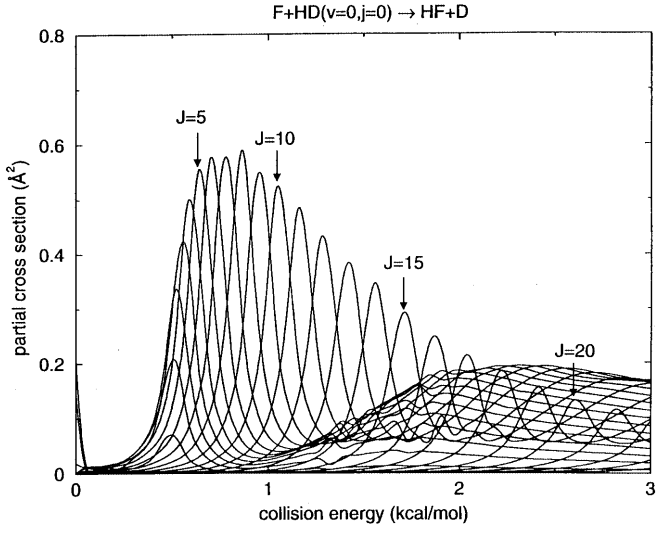

Fig. 3. Computed partial cross sections for the F + HD($v = 0$, $j = 0$) $\rightarrow$ HF + D reaction as a function of the total angular momentum quantum number, J, up to collision energies of 3 kcal mol^{-1}

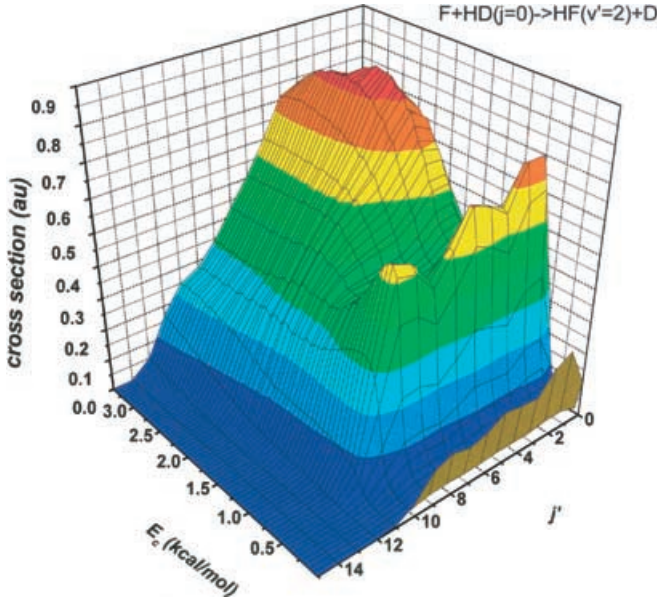

Fig. 4. The integral cross sections (*ICS*) for F + HD($v = 0$, $j = 0$) $\rightarrow$ HF($v' = 2$, j') + D versus E_C and j' computed from quantum scattering theory using the SW-PES

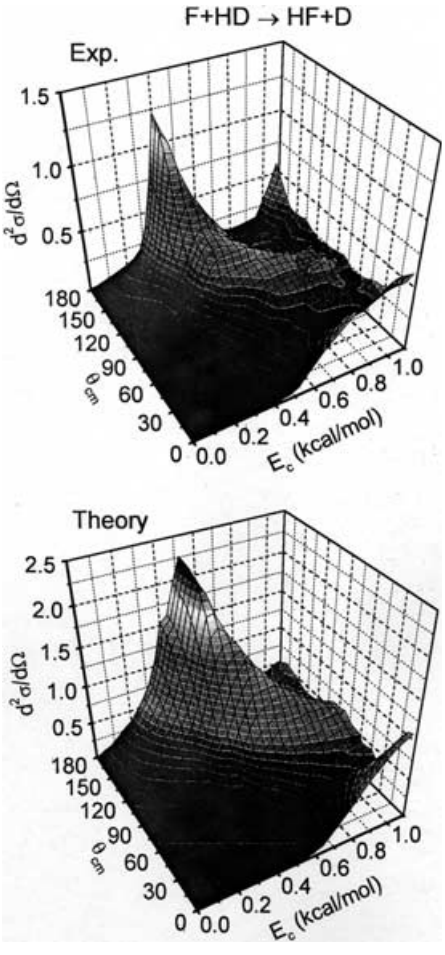

Fig. 5. The total differential cross section (*DCS*) (Å^{2}sr^{-1}) for the F + HD $\rightarrow$ HF($v' = 2$) + D reactive channel. The *upper panel* shows the experimental results, while the *lower panel* presents the result of the scattering calculation. Note the ridge running from large θ (backward) at low energies to small θ (sideways) at higher E_C

position of the DCS into resonant and direct components, by fitting each **S**-matrix element to a Breit–Wigner pole plus a background, verifies that this peaking is in fact due primarily to the resonant contribution [56].

To uniquely associate the unusual behavior of the collision observables with the existence of a reactive resonance, it is necessary to theoretically characterize the quantum state that gives rise to the Lorentzian profile in the partial cross sections. Using the method of SQ, it is possible to extract a Seigert state wavefunction from time-dependent quantum wavepackets using the Fourier relation

$$\Psi_{\mathrm{res}} \propto \int_{-\infty}^{\infty} \phi(t) \exp(iE_{\mathrm{res}}t/\hbar)\mathrm{d}t \ , \qquad (3.3)$$

where E_{res} is taken to be the resonance energy (peak position of the Lorentzian). In SQ, the background direct reaction contribution to the time-independent wavefunction (always present when using Eq. 3.3) can be suppressed by variationally choosing the initial wavepacket $\phi(0)$ to minimize the direct contribution, thus yielding a pure resonance state wavefunction. The state obtained in this way for $J = 0$ is shown in Fig. 6; this state is localized in the collinear F–H–D arrangement with three quanta of excitation in the asymmetric stretch mode, and zero quanta of excitation in the bend and symmetric stretch modes. If the state pictured in Fig. 6 is used as an initial (prepared) state in a wavepacket calculation, one observes a pure exponential decay with a lifetime of 109 fs, consistent with the width of the Lorentzian peak in the partial cross section. Furthermore, the product state distribution of the decaying resonance is consistent with the results of the scattering calculations for $E_{\mathrm{C}} < 1$ kcal mol^{-1}. Takayanagi and Wada [64] performed a stabilization calculation that confirmed the existence of the resonance state on the SW PES.

Finally, quantum mechanical trapping at the resonance energy can be verified using a time-delay analysis on the quantum **S** matrix. The average time delay for the $J = 0$ partial wave of the F + HD $\rightarrow$ HF + D reaction, defined using the diagonal Smith lifetime matrix [43], is plotted in Fig. 7 versus the collision energy. A clear peak in the time delay is observed near the resonance energy. Higher partial waves exhibit similar behavior, with the peak of the time delay J-shifting according to Eq. (3.1).

In summary, the reactive resonance for the F + HD $\rightarrow$ HF + D reaction is found to leave clear signatures on a variety of collision observables. The resonance state itself is readily extracted from the quantum dynamics on the SW PES, and the scattering observables are found to correlate well with the predictions of theory.

3.2 F + H_2, an experiment waiting to be done

A resonance phenomenon in the F + H_2 system was predicted [65, 66] in the early 1970s on the basis of theoretical modeling of the collinear reaction dynamics employing the Muckerman-5 empirical PES [67]. The

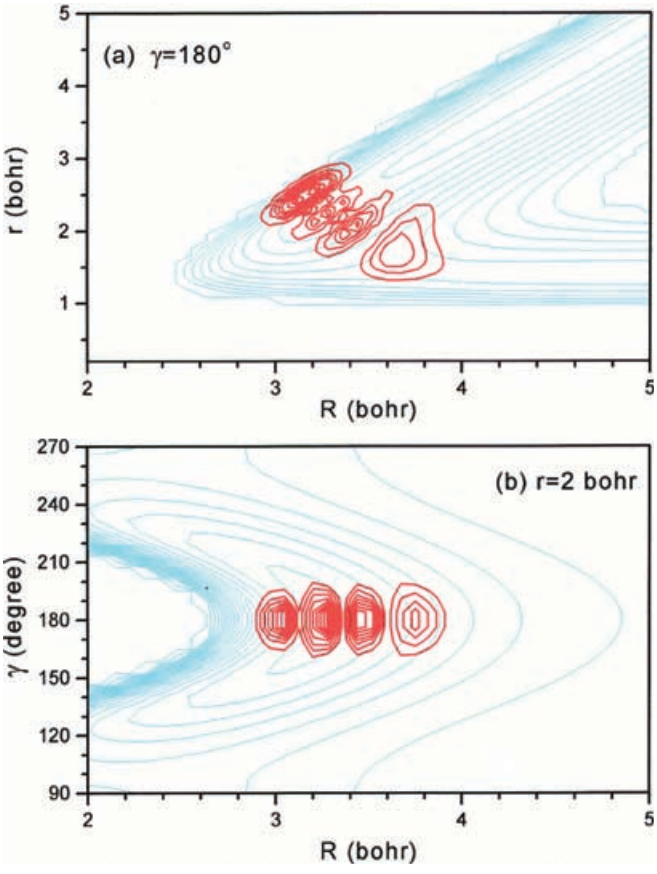

Fig. 6a,b. The probability density of the reactive resonance at $E_{\mathrm{C}} = 0.52$ kcalmol^{-1}. **a** The probability density in the F–H–D collinear subspace using the reactant channel Jacobi coordinates (R, r). **b** The probability density is sliced at $r = 2$ bohr and is shown in the Jacobi (R, γ) coordinates. The plot clearly shows a state with three nodes along the asymmetric stretch and zero nodes in the symmetric stretch and bend

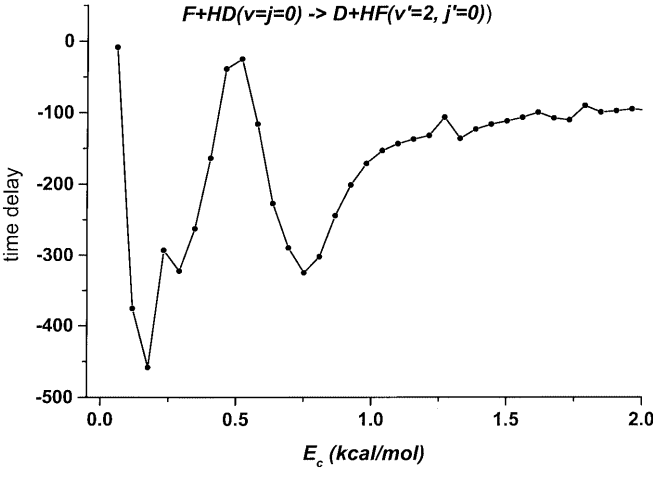

Fig. 7. The time delay versus E_{C} for the reaction F + HD(0, 0) $\rightarrow$ D + HF($v' = 2$, $j' = 0$) with $J = 0$. The time delay was computed using Wigner's definition

case for a reactive resonance was strongly bolstered by the molecular beam experiments of Neumark et al. [49], who observed an anomalous forward peak in the

angular distribution of the HF($v' = 3$) product state. However, the issue was thrown into some doubt when the quantum scattering calculations on the accurate SW PES failed to yield a clear resonance signature in the quantum time delay [68]. Furthermore, QCT calculations [61] also revealed a forward peak in the HF($v' = 3$) product, which seemed to suggest that the hypothesis of a quantum scattering resonance was not necessary to explain the experiment. A direct measurement of the transition-state spectrum using anion photodetachment by Manolopoulos et al. [69] was finally assigned to van der Waals states without the need for transition-state resonances.

The excitation function for the F + $H_2 \rightarrow$ HF + H reaction was recently measured by Dong et al. [70] in a molecular beam apparatus over the range of collision energies 0.1–3.0 kcal mol^{-1} for both normal- and *para*-H_2 reagent. Unlike the F + HD reaction, no clear resonance step was apparent in $\sigma_R(E)$. However, there was a significant difference between the H_2(n) and H_2(p) reactivity, implying a fairly strong dependence on the reagent rotational state. As seen in Fig. 8, the quantum scattering calculations of Chao and Skodje [71] are in reasonable agreement with experiment, although some inaccuracies in the SW PES are apparent. However, the theory does yield a small double-step feature in $\sigma_R(E)$ for H_2(p) beginning at $E_C = 0.34$ kcal mol^{-1} that was too faint to resolve in the beam experiment. The partial cross sections for the individual partial waves, shown in Fig. 9, reveal that the double step in $\sigma_R(E)$ is the by-product of two Lorentzian peaks spaced by about 0.3 kcal mol^{-1}. These peaks move closer together as J is increased, until they merge into a single peak for $J > 10$. The effective B constants obtained by fitting the two peak energies to Eq. (3.1) imply that the geometry of the lower-energy peak is consistent with the transition state, while the higher-energy peak gives a smaller B constant more in keeping with the geometry of the minimum of the van der Waals well in the H–HF channel. Thus,

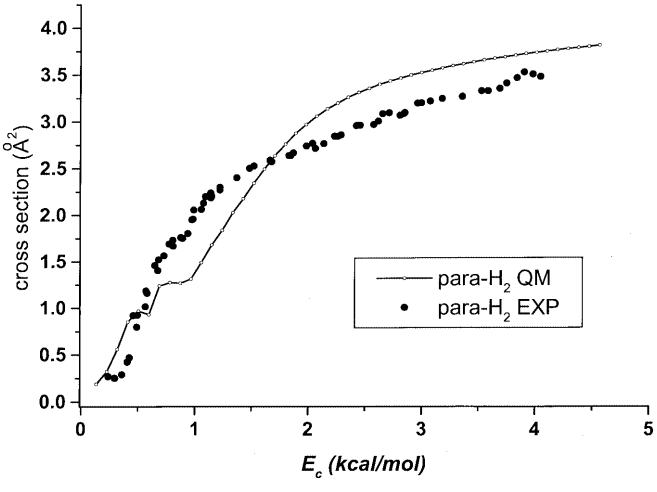

Fig. 8. The excitation function (Å^2) for the reaction F + H_2(p) $\rightarrow$ H + HF versus collision energy. The *solid line* is the result of quantum scattering calculations done with the SW-PES and the *points* are the molecular beam experiments

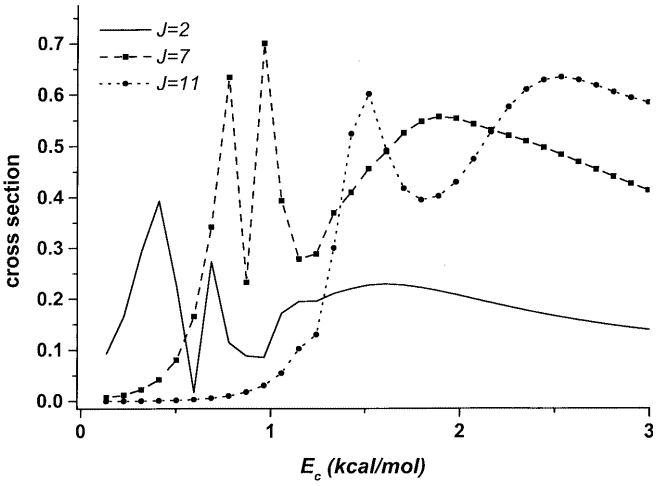

Fig. 9. The partial cross section summed over all final states (Å^2) for F + $H_2(0, 0) \rightarrow$ H + HF at several values of the total angular momentum J. The partial cross section shows a double-peak structure which J-shifts to higher energy with J, and eventually merges at about $J = 10$

while some hint of resonant behavior in $\sigma_R(E)$ may exist, the effect is too small to be clearly seen in the experiment.

The origin of the double-peak structure in the partial cross sections was clearly established by use of the SQ procedure [71]. It was found that the lower-energy peak was due to a reactive resonance with an identical mode assignment as for F + HD with $E_R(J = 0) = 0.34$ kcal mol^{-1} and $\Gamma = 0.26$ kcal mol^{-1}, while the higher peak was assigned to the H–HF($v' = 3, j' = 0$) van der Waals state at 0.62 kcal mol^{-1} [72]. The complexity of the F + H_2 reaction, compared to F + HD, is largely the result of the overlapping (and interfering) contributions of these two states in the collision observables. In contrast, for the F + HD reaction, the corresponding D–HF($v' = 3, j' = 0$) state lies at 1.31 kcal mol^{-1}, which is high enough not to interfere with the resonance contribution.

While it is clear that a resonance does exist for F + H_2 on the SW PES, many of the INR probes for resonant behavior fail. As already noted, Castillo et al.[68] did not detect a peak in the time-delay function at the resonance energy. We have reproduced that calculation using a finer energy grid in Fig. 10. At the purported resonance energy, $E_C = 0.34$ kcal mol^{-1}, a vague shoulder is seen in the time delay rather than a clear peak. Obviously complicating the analysis, however, is the rapidly varying "background" time delay, which is reflecting the nearby energetic threshold to reaction. Similarly, the calculated rotational product state distributions, shown in Fig. 11, show no clear imprints of the resonance behavior. Any unusual rotational signatures from the nascent resonance decay are apparently damped by passage through the van der Waals region.

As presaged by Neumark et al. [49], it is in the angular distributions that the clearest sign of resonance behavior is observed. We plot the calculated DCS versus E_C and θ for F + H_2(p) $\rightarrow$ HF($v' = 2$) + H summed over j′ states in Fig. 12. Near the resonance energy, we

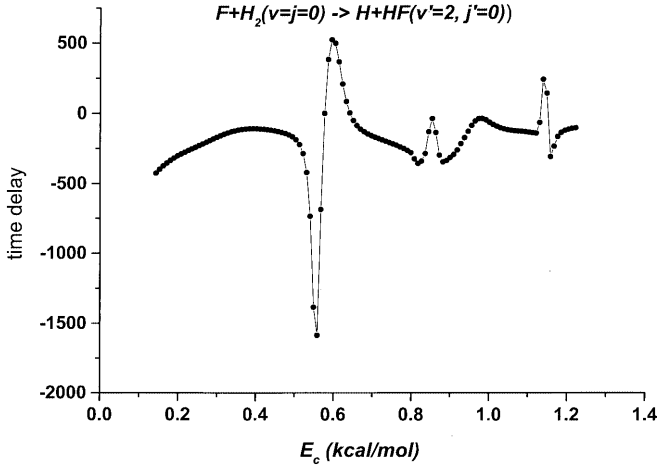

Fig. 10. The (Wigner) time delay versus E_C for the reaction F + $H_2(0, 0) \rightarrow$ H + HF($v' = 2$, $j' = 0$) with $J = 0$, where the same expression used for F + HD was employed

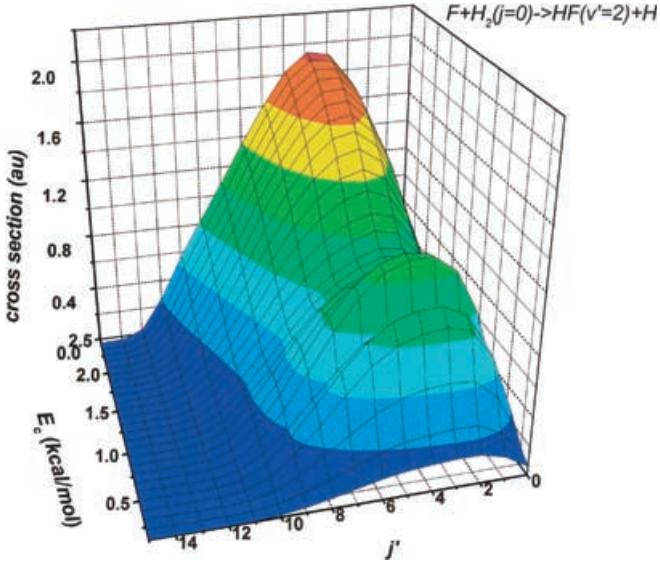

Fig. 11. The ICS for F + $H_2(v = 0, j = 0) \rightarrow$ H + HF($v' = 2$, j') versus E_C and j' computed from quantum scattering theory using the SW-PES

observe a very dramatic change in the angular product distribution. At $E_C = 0.34$ kcal mol^{-1} the DCS is backward-peaked, at $E_C = 0.55$ kcal mol^{-1} it swings to the forward direction, then again by $E_C = 0.8$ kcal mol^{-1} it shifts again to the backward direction. This very pronounced oscillation in the DCS is the result of interference between contributions from the reactive resonance and the van der Waals state. At higher energies, such as those considered by Neumark et al., the resonance contributions to the DCS are most apparent in the forward scattering direction.

Unfortunately, the experimental confirmation of the dramatic energy/angle correlations predicted by theory has not yet been obtained in the laboratory. Lee and Liu did not obtain the DCS in the critical 0.2–1.0 kcal mol^{-1} range of collision energies. An experimental determination of the DCS on a fine grid of energies would be quite

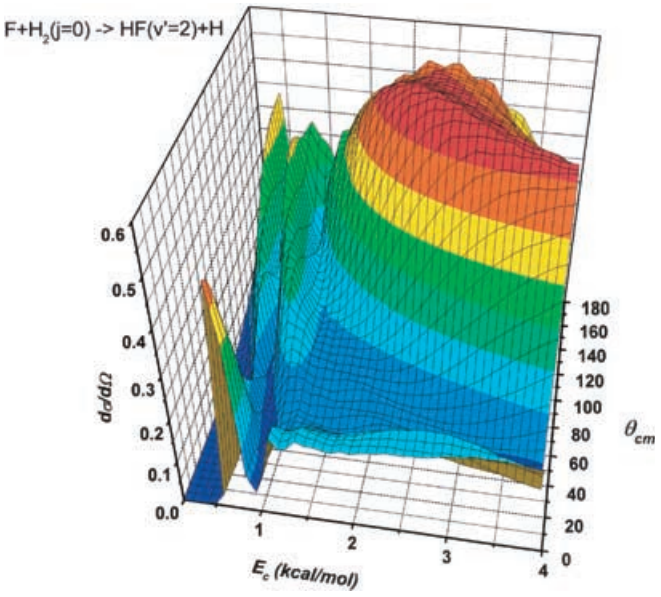

Fig. 12. The DCS (Å^{2}sr^{-1}) for F + $H_2(v = 0, j = 0) \rightarrow$ H + HF($v' = 2$, $j' =$ all). Notice the strong energy–angle correlation at low collision energy

useful, both as a confirmation of the theory and for new information about the PES. It is our experience that the details of the DCS are extremely sensitive to the PES. Indeed, we expect that errors as small as 0.1 kcal mol^{-1} in the PES would be apparent from disagreements between theory and experiment.

3.3 The H + HD system

The search for reactive resonances in the H + H_2 reaction (and its isotopomers) has a long history [2, 3, 4, 5, 73]. The existence of resonances was first conjectured on the basis of theoretical collinear quantum dynamics simulations using approximate PESs [6, 7, 8, 9]. Subsequent improvements in theory, such as the use of a very accurate PES and the implementation of full 3D dynamics, strongly implied that the resonances should actually exist in the ''real'' system [12, 13, 14]. Despite the simplicity of this reaction, it has only been rather recently that ab initio theoretical reaction dynamics has been brought into agreement with state-resolved experimental results [74, 75, 76]. Nevertheless, clear signatures of resonant behavior have proven to be very difficult to identify in experiment, and several false sightings have been reported. By any measure, the experimental conditions required for the measurements are quite rigorous. The resonances are predicted to exist at high E_C, requiring hot-atom beam sources such as HI photolysis products for which it is difficult to obtain a well-calibrated energy-tunable beam. Furthermore, the resonances will probably have very short lifetimes (about 20 fs) and thus will display very large widths as a function of collision energy, about 0.5 kcal mol^{-1}. Therefore, it becomes a subtle matter to distinguish between the direct and resonance contributions to the scattering cross sections. Further complicating the

analysis is the possible influence of the geometrical phase [77] that might have significant effects on the resonance properties, as stressed by Kuppermann and Wu [78] Weak undulations in certain state-resolved ICS versus E_C for H + D_2 have been predicted by Chao and Skodje [79], but are likely to be at or below the detection threshold. These undulations, seen most strongly for the ICS $\sigma_R(00 \rightarrow 00)$ and $\sigma_R(00 \rightarrow 02)$, are problematic as resonance fingerprints since they are not uniquely correlated to the barrier states of the reaction. [Here we use the notation $\sigma_R(vj \rightarrow v'j')$.] Fernandez-Alonso et al. [51] have observed a forward peak in the H + D_2 DCS, which is consistent with a resonance picture. Theoretical simulations have, in fact, demonstrated that the forward peak does exhibit extra time delay in line with the physical picture outlined earlier [80].

Here we consider the H + HD $\rightarrow$ D + H_2 reaction, which has recently been studied experimentally and theoretically by Harich et al. [54]. The reaction was investigated experimentally in a crossed-molecular-beam apparatus employing the D-atom Rydberg tagging detection scheme originally proposed by Schneider and coworkers[74]. The hot H-atom beam source was provided by HI photolysis that produced two well-separated collision energies, $E_C = 0.499$ and 1.200 eV. The initial HD beam was cooled to the point where only the ground state, HD(0, 0), was represented in the beam. The state-resolved DCS were obtained for all the important ro-vibrational product channels. The theoretical analysis involved QCT, quantum scattering, and wavepacket calculation on the accurate BKMP2 PES [81] but without the geometrical phase.

The ICS for several channels are plotted in Fig. 13 versus total energy, $E = E_C + 0.235$ eV, which includes the zero-point energy. The experiment (results plotted with symbols) and theory are in good agreement, but show no clear sign of resonance behavior over the energy range considered. Although the underlying reaction probabilities $P_R(v, j \rightarrow v', j'; E_C, J)$ do exhibit modest oscillation versus E_C, the impact parameter averaging effectively washes out this structure in the cross sections. Similarly, the j' dependence of the D + $H_2(v' = 0, j')$ products (Fig. 14) show no unusual energy dependence of the sort seen previously for F + HD. We note parenthetically, however, that there is a dramatic effect of spin statistics that causes the distributions to exhibit a saw-toothed dependence on j'. The state resolved DCS for several states is shown in Fig. 15. Several of the DCS show weak vestiges of the resonance ridge, such as the $d\sigma_R(0, 0 \rightarrow 0, 0)/d\Omega$. The ridges in these cases are clearly associated with the maximum of the ground adiabatic potential (i.e., the lowest barrier state) and not with any higher-lying Feshbach-type resonance. The most dramatic effect in the angular distributions is the presence of a strong and very narrow forward scattering peak in the DCS for low rotational product states. This forward peak was observed in both the theoretical and the experimental results. As seen in Fig. 15, the forward peak for the $(0, 0 \rightarrow 0, 0)$ case begins at about $E_C = 1$ eV and persists to the highest energies considered. Other final rotational states likewise show a forward peak, but at progressively higher energies.

The results indicate that the strongest case for reactive resonances in the H + HD reaction is to be found in the forward peaking of the DCS. To establish the link between the forward peak and resonance behavior, it is necessary to analyze the underlying reaction dynamics that gives rise to the forward peaking. First, as noted in other reactions, the forward peak is the by-product of high-impact-parameter (i.e., high J) reactive scattering. As an illustration, in Fig. 16 we plot the forward scattering integrated opacity function $d\sigma_R(00 \rightarrow 00; \theta = 0, E_C, J_{max})$ versus J_{max} at the experimental collision energy of $E_C = 1.200$ eV. In this quantity, the DCS is

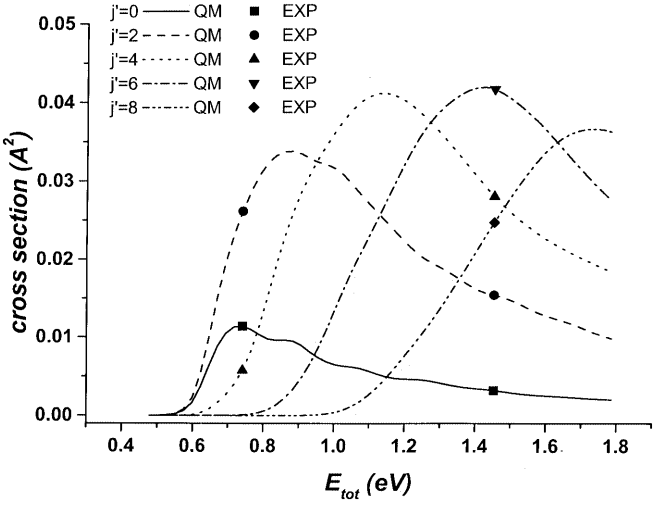

Fig. 13. The ICS for H + HD($v = 0, j = 0$) $\rightarrow$ D + $H_2(v' = 0, j')$ versus total energy for several final rotational channels. The *curves* are obtained from quantum scattering theory, while the *symbols* are experimental results

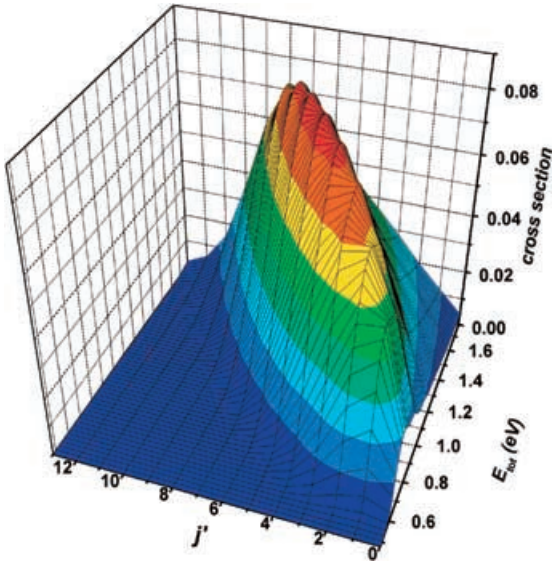

Fig. 14. The ICS for H + HD($v = 0, j = 0$) $\rightarrow$ D + H_2 ($v' = 0, j'$) versus E_C and j' computed from quantum scattering theory using the BKMP2 PES. To aid visualization, the results are shown using Boltzmann statistic for H_2 product

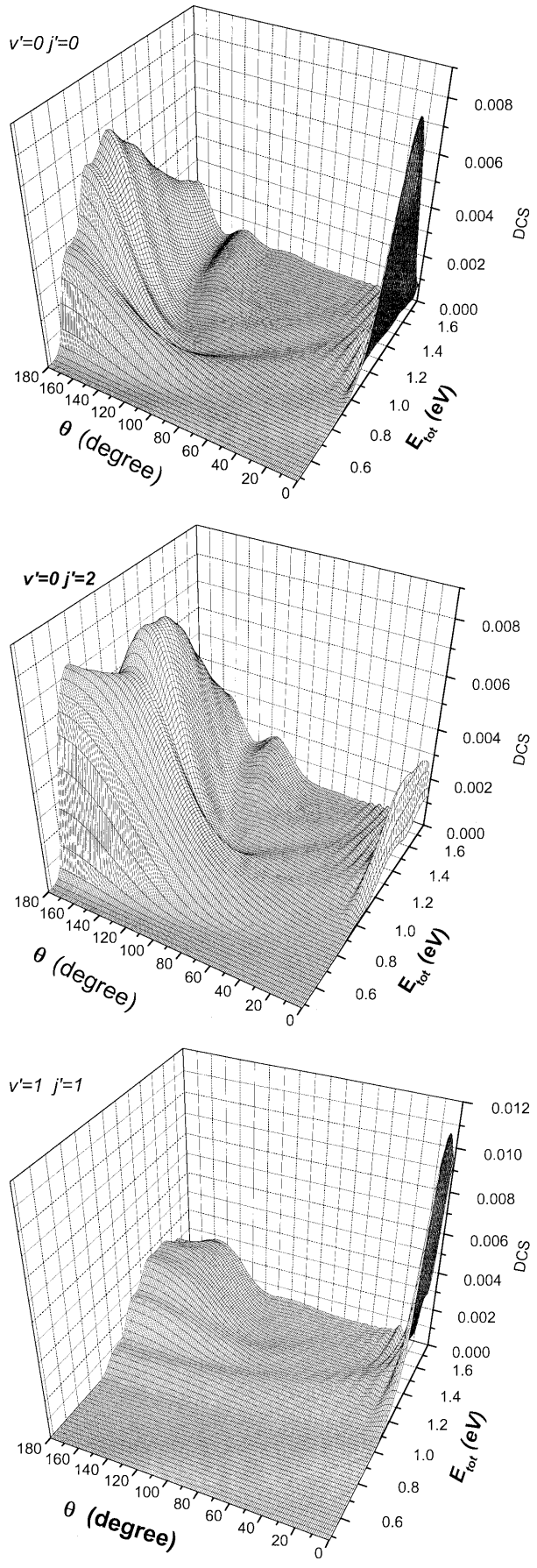

Fig. 15. The DCS ($Å^2 sr^{-1}$) for the several final states of the H + HD($v = 0, j = 0$) → D + $H_2(v', j')$ reaction. The results were computed from quantum scattering theory using the BKMP2 PES

computed only using partial waves up to J_{max}. As seen in the figure, the forward peak comes from just a small number of partial waves near the value $J_{max} = 25$; at this value of J, the vibrationally adiabatic barriers are centrifugally shifted upward by about 0.5 eV relative to the nonrotating barriers. Next, we note that the forward scattering peak is rotationally cold and vibrationally hot compared to scattering in other directions. By averaging the DCS over the narrow interval $\theta = [0–5°]$, it is found that $\langle j' \rangle_{\theta=0} = 1.3$ and $\langle E'_{vib} – E_{H_2}(v' = 0, j' = 0) \rangle_{\theta=0} = 1{,}155\ cm^{-1}$. These numbers can be contrasted with the ICS results that average over all scattering angles, $\langle j' \rangle_{all} = 5.3$ and $\langle E'_{vib} – E_{H_2}(v' = 0, j' = 0) \rangle_{all} = 574\ cm^{-1}$. In Fig. 17, we plot the mean product vibrational energy versus scattering angle for H + HD(0, 0) → D + $H_2(v', j')$ at $E_C = 1.200$ eV, which clearly reveals the special product distribution in the forward direction. Finally, to connect the forward scattering to dynamical trapping phenomena, we consider the behavior of the angle-dependent time-delay. The j'-averaged time delay for H + HD(0, 0) → D + $H_2(v' = 0)$ is plotted versus the scattering angle at $E_C = 1.200$ eV in Fig. 18. The forward direction is seen to exhibit a time delay about 20 fs longer than the other scattering directions.

The state assignment of resonance which gives rise to the forward peaking is a delicate issue. It is clear from Fig. 16 that the state involved is highly rotationally excited; thus, the resonance states are distorted from their $J = 0$ counterparts. However, it is possible to demonstrate on energetic grounds that the $J = 25$ resonance corresponds to the adiabatic barrier maximum of two internal states of the H–H–D complex, viz., the (v_{ss},

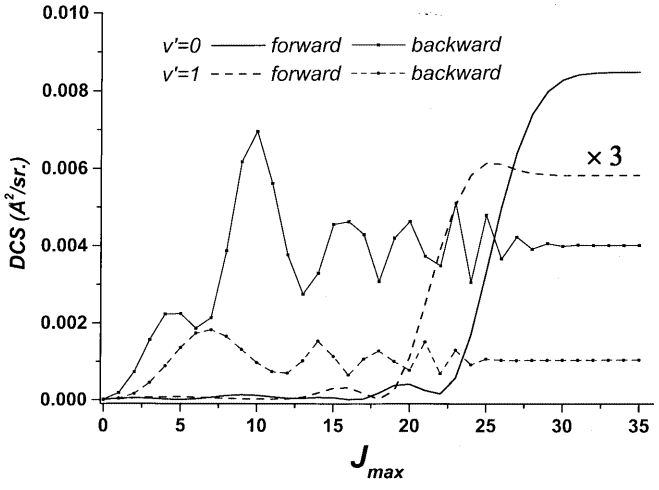

Fig. 16. The angle-dependent integrated opacity function $d\sigma_R$ ($00 \rightarrow v'j'$; θ, E_C, J_{max}) versus J_{max} computed at the experimental energy $E_C = 1.200$ eV for the cases (v', j') = (0, 0) and (1, 0). This quantity is computed by restricting the partial wave sum in the DCS to the terms $J = J_{max}$. The result is shown for both forward and backward scattering to illustrate the J contributions to scattering at different θ

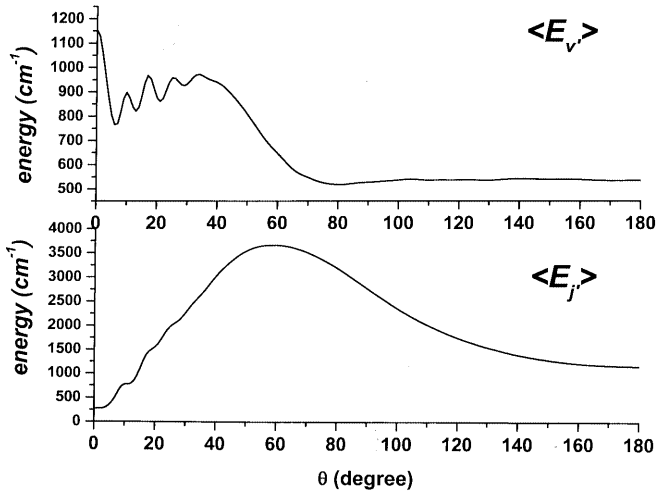

Fig. 17. The average product rotational and vibrational excitation versus scattering angle for H + HD($v = 0$, $j = 0$) → D + H_2 at $E_C = 1.200$ eV computed by quantum scattering theory

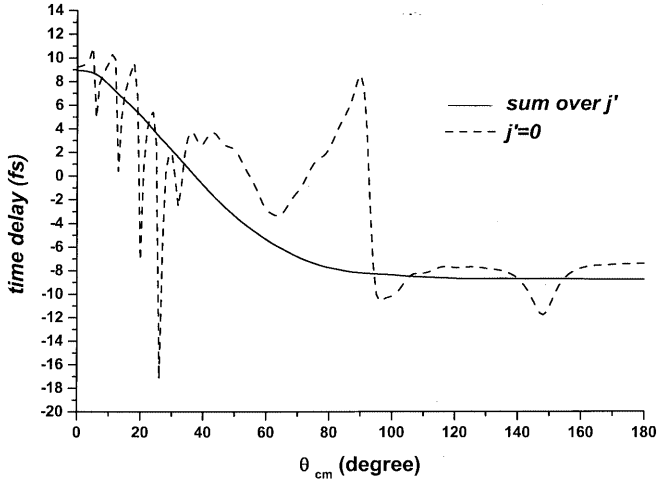

Fig. 18. The scattering time delay versus θ for H + HD($v = 0$, $j = 0$) → D + H_2 at $E_C = 1.200$ eV. The *dashed curve* is obtained using the formula of Goldberger and Watson for the final state $H_2(v' = 0, j' = 0)$, while the *solid line* is the result of averaging over the final rotational states, j' for the dominant $v' = 0$ product. Both curves show roughly an extra 20 fs of time delay in the forward direction, but the averaging eliminates the spurious structures that are related to minima in the DCS versus θ

$v_{bend}) = (1, 0)$ and $(0, 2)$. Since neither adiabatic potential curve, $V_{ad}(s; 1, 0)$ nor $V_{ad}(s; 0, 2)$, exhibits sufficiently deep wells to trap a Feshbach resonance at $J = 25$, the resonance state is a barrier state. Because of the near degeneracy of the two barrier heights, the trapping will involve a combination of symmetric stretch and bend excitations at the transition state.

In summary, the H + HD reaction shows little sign of resonance scattering in the ICS. Furthermore, the product distributions without angle resolution show no unusual behavior as functions of energy that might indicate resonance behavior. On the other hand, the forward peaking in the angular product distribution does appear to reveal resonance structure. Since time-delay analysis is at present not possible in a molecular beam experiment, it is the combination of a sharp forward peak with the unusual angular product distribution that most clearly indicates the presence of a resonance.

4 Conclusions

The field of gas-phase reaction dynamics has reached a level of maturity where many of the fundamental, and motivating, questions about the nature of reactive collisions can finally be answered. The role of short-lived resonance states in understanding reaction dynamics is an essential one. As we have seen, resonances can have a dramatic influence on physical observables such as excitation functions, state-to-state branching ratios, and angular product distributions. Even highly averaged quantities, like the low-temperature reaction rate constant for F + HD → D + HF, can be strongly affected by processes such as resonance tunneling. Thus, it is clear that many of the basic observables obtained in modern reaction kinetics experiments cannot be fully understood without reference to resonance phenomena. Moreover, the study of reactive resonances also provides a window to observe the dynamics occurring in the crucial transition-state region. The resonance properties, such as energy and lifetime, provide sensitive probes of the PES near the saddle point. Indeed, the comparison of experiment to converged dynamics calculations then provides a working definition of "chemical accuracy" for quantum chemistry calculations, which shall be the most rigorous in treating resonant scattering.

It would be gratifying to provide future researchers with a unique and unmistakable resonance signature which could applied to new and more complicated chemical reactions. Unfortunately, at this point, it seems that resonance signatures are as diverse as the reactions themselves. It is clear, however, that a strong interplay between theory and experiment will always be required.

Acknowledgements. For their valuable input into the research discussed here, we are grateful to our collaborators, K. Liu, S.H. Lee, F. Dong, D.E. Manolopoulos, D, Skouteris, X. Yang, S. Harich, D. Dai, and C.C. Wang. This work was supported by the National Science Foundation.

References

1. Levine RD, Bernstein RB (1987) Molecular reaction dynamics and chemical reactivity. Oxford University Press, New York
2. Kuppermann A (1981) In: Truhlar DG (ed) Potential energy surfaces and dynamics calculations. Plenum, New York, p 375
3. Garrett BC, Schwenke DW, Skodje RT, Thirumalai D, Thompson TC, Truhlar DG (1984) ACS symposium series 263. American Chemical Society, Washington, DC, pp 375–400
4. Liu K (2001) Annu Rev Phys Chem 52: 139
5. Fernandez-Alonso F, Zare RN (2002) Annu Rev Phys Chem 53: 67
6. Truhlar DG, Kuppermann A (1970) J Chem Phys 52: 3841
7. Truhlar DG, Kuppermann A (1972) J Chem Phys 56: 2232
8. Levine RD, Wu S-F (1971) Chem Phys Lett 11: 557
9. Wu S-F, Levine RD (1971) Mol Phys 22: 881
10. Schatz GC, Kuppermann A (1973) J Chem Phys 59: 964

11. Schatz GC, Kuppermann A (1975) Phys Rev Lett 35: 1266
12. Zhao MS, Mladenovic M, Truhlar DG, Schwenke DW, Sharafeddin O, Yan Y, Kouri DJ (1989) J Chem Phys 91: 5302
13. Cuccaro SA, Hipes PG, Kuppermann A (1989) Chem Phys Lett 157: 440
14. Skodje RT, Sadeghi R, Koppel H, Krause JL (1994) J Chem Phys 101: 1725
15. Gray SK (1992) J Chem Phys 96: 6543
16. (a) Sadeghi R, Skodje RT (1993) J Chem Phys 98:9208; (b) Sadeghi R, Skodje RT (1993) J Chem Phys 99: 5126
17. Sadeghi R, Skodje RT (1995) J Chem Phys 102: 193
18. Jolicard G, Leforestier C, Austin EJ (1988) J Chem Phys 88: 1026
19. Mandelstam V, Taylor HS (1997) J Chem Phys 107: 5756
20. Neumark DM (1992) Annu Rev Phys Chem 43: 153
21. Weaver A, Metz RB, Bradforth SE, Neumark DM (1988) J Phys Chem 92: 5558
22. Miller WH, Handy NC, Adams JE (1980) J Chem Phys 72: 99
23. Isaacson AD, Truhlar DG (1982) J Chem Phys 76: 1380
24. Friedman RS, Truhlar DG (1991) Chem Phys Lett 183: 539
25. Chatfield DC et al (1996) In: Wyatt RE, Zhang JZH (eds) Dynamics of molecules and chemical reactions. Dekker, New York, p 323
26. Pollak E, Pechukas P (1978) J Chem Phys 69: 1218
27. Zobay O, Alber G (1993) J Phys B 26:L539
28. Burhardt I, Gaspard P (1994) J Chem Phys 100: 6395
29. Seideman T, Miller WH (1991) J Chem Phys 95: 1768
30. Ryaboy V, Moiseyev N (1993) J Chem Phys 98: 9618
31. Sadeghi R, Skodje RT (1995) Phys Rev A 52:1996
32. (a) Reinhardt WP (1982) Annu Rev Phys Chem 33: 223; (b) Hazi AU, Taylor HS (1970) Phys Rev A 1: 1109
33. Thompson TC, Truhlar DG (1984) J Phys Chem 88: 210
34. Skokov S, Bowman JM (1999) J Chem Phys 111: 4933
35. Maiti B, Mahapatra S, Sathyamurthy N (2000) J Chem Phys 113: 59
36. Varandas AJC, Yu HG (1996) Chem Phys 209: 31
37. Goldberger ML, Watson KM (1964) Collision theory. Wiley, New York
38. Breit G, Wigner EP (1936) Phys Rev 49: 519
39. Taylor JR (1972) Scattering theory. Wiley, New York
40. Seigert AJ (1939) Phys Rev 56: 750
41. Miller WB, Safron SA, Herschbach DR (1967) Discuss Faraday Soc 44: 108
42. (a) Wigner EP (1955) Phys Rev 98:145; (b) Eisenbud L ( ) PhD thesis. Princeton University
43. Smith FT (1960) Phys Rev 118: 349
44. (a) Goldberger ML, Watson KM (1964) Collision theory. Wiley, New York, p 494; (b) Goldberger ML, Watson KM (1962) Phys Rev 127:2284; (c) Froissart M, Goldberger ML, Watson KM (1963) Phys Rev 131: 2820
45. Kuppermann A, Wu Y-S (1995) Chem Phys Lett 241: 229
46. Redmon MJ, Wyatt RE (1979) Chem Phys Lett 63: 209
47. Miller WH, Zhang JZH (1991) J Phys Chem 95: 12
48. (a) Aoiz FJ, Herrero VJ, Rabanos VS (1991) J Chem Phys 95: 7767; (b) Aoiz FJ, Herrero VJ, Rabanos VS (1991) J Chem Phys 97: 7423
49. Neumark DM, Wodke AM, Robinson GN, Hayden CC, Shobatake R, Lee YT (1985) J Chem Phys 82: 3045
50. Neumark DM, Wodke AM, Robinson GN, Hayden CC, Shobatake R, Sparks RK, Schafer TP, Lee YT (1985) J Chem Phys 82: 3067
51. Fernandez-Alonso F, Bean BD, Ayers JD, Pomerantz AE, Zare RN, Banares L, Aoiz FJ (2000) Angew Chem Int Ed Engl 39: 2748
52. (a) Fernandez-Alonso F, Bean BD, Zare RN (1999) J Chem Phys 111: 1022; (b) Fernandez-Alonso F, Bean BD, Zare RN (1999) J Chem Phys 111: 2490; (c) Fernandez-Alonso F, Bean BD, Zare RN, Aoiz FJ, Banares L, Castillo JF (2001) J Chem Phys 114: 4534
53. Bean BD, Ayers JD, Fernandez-Alonso F, Zare RN (2002) J Chem Phys 116: 6634
54. (a) Harich SA, Dai DX, Wang CC, Yang X, Chao SD, Skodje RT (2002) J Chem Phys 116: 4769
54. (b) ibid (2002) Nature 419: 281
55. Skodje RT, Skouteris D, Manolopoulos DE, Lee S-H, Dong F, Liu K (2000) J Chem Phys 112: 4536
56. Skodje RT, Skouteris D, Manolopoulos DE, Lee S-H, Dong F, Liu K (2000) Phys Rev Lett 85: 1206
57. Liu K, Skodje RT, Manolopoulos DE (2002) Phys Chem Commun 4
58. (a) Castillo JF, Manolopoulos DE (1998) Faraday Discuss 110: 119; (b) Castillo JF, Manolopoulos DE (1998) Faraday Discuss 110: 213
59. Stark K, Werner H-J (1996) J Chem Phys 104: 6515
60. Skouteris D, Castillo JF, Manolopoulos DE (2000) Comput Phys Commum 133: 128
61. (a) Aoiz FJ, Banares L, Herrero VJ, Rabanos VS, Stark K, Werner H-J (1994) Chem Phys Lett 223:215; (b) (1995) J Chem Phys 102:
62. Schatz GC, Sokolovski D, Connor JNL (1991) J Chem Phys 94: 4311
63. Harper WW, Nizkorodov SA, Nesbitt DJ (2002) J Chem Phys 116: 5622
64. Takayanagi T, Wada A (2001) Chem Phys Lett 348: 524
65. Wu SF, Johnson BR, Levine RD (1973) Mol Phys 25: 839
66. Schatz GC, Bowman JM, Kuppermann A (1975) J Chem Phys 63: 674
67. Muckerman JT (1981) In: Eyring H, Henderson D (eds) Theoretical chemistry – advances and perspectives, vol 6A. Academic, New York, p 1
68. Castillo JF, Manolopoulos DE, Stark K, Werner H-J (1996) J Chem Phys 104: 6531
69. Manolopoulos DE, Stark K, Werner H-J, Arnold DA, Bradforth SE, Neumark DM (1993) Science 262: 1852
70. Dong F, Lee SH, Liu K (2000) J Chem Phys 113: 3633
71. Chao SD, Skodje RT (2000) J Chem Phys 113: 3487
72. Takayanagi T, Kurosaki Y (1998) J Chem Phys 109: 8929
73. Miller WH (1990) Annu Rev Phys Chem 41: 245
74. (a) Schnieder L, Seekamp-Rahn K, Borkowski J, Wrede E, Welge KH, Aoiz FJ, Banares L, D'Mello MJ, Herrero VJ, Saez Rabanos V, Wyatt RE (1995) Science 269: 207; (b) Schnieder L, Seekamp-Rahn K, Wrede E, Welge KH (1997) J Chem Phys 107: 6175; (c) Wrede E, Schnieder L, Welge KH, Aoiz FJ, Banares L (1996) J Chem Phys 106: 7862
75. Kitsopoulos TN, Buntine MA, Baldwin DP, Zare RN, Chandler DW (1993) Science 260: 1605
76. Harich SA, Dai DX, Wang CC, Yang X, Chao SD, Skodje RT (2002) J Chem Phys (in press)
77. Mead CA, Truhlar DG (1979) J Chem Phys 70: 2284
78. (a) Kuppermann A, Wu Y-SM (1993) Chem Phys Lett 205: 577; (b) Kuppermann A, Wu Y-SM (1993) Chem Phys Lett 349: 537
79. Chao SD, Skodje RT (2001) Chem Phys Lett 336: 364
80. Althorpe SC, Fernandez-Alonso F, Bean BD, Ayers JD, Pomerantz AE, Zare RN, Wrede E (2002) Nature 416: 67
81. Boothroyd AI, Keogh WJ, Martin PG, Peterson MR (1996) J Chem Phys 104: 7139